Schweizerischer Erdbebendienst
Service Sismologique Suisse
Servizio Sismico Svizzero
Servizi da Terratrembels Svizzer

Eidgenössische Technische Hochschule Zürich
Swiss Federal Institute of Technology Zurich

Zürich - Zeughaushof (SZUZ)

SITE CHARACTERIZATION REPORT

Clotaire MICHEL, Carlo CAUZZI, Daniel ROTEN

Valerio POGGI, Jan BURJANEK, Donat FÄH

Sonneggstrasse 5 CH-8092 Zürich Switzerland; E-mail: clotaire.michel@sed.ethz.ch

Last modified : November 5, 2013

Abstract

Ambient vibration array measurements were performed to characterize the site Zürich Zeughaushof. The site, where the new station SZUZ of the Swiss Strong Motion Network was installed, is located in the Limmat basin. In order to characterize the velocity profile under the station, array measurements with a $300\,\mathrm{m}$ aperture were performed. The measurements were successful and allowed deriving a velocity model for this site. The soil column underlying station SZUZ is made of a first layer of approximately $10\,\mathrm{m}$ with velocities from 250 to $500\,\mathrm{m/s}$ corresponding to recent fluvial sediments and washed moraine. It is responsible for a peak in the ellipticity around $10\,\mathrm{Hz}$. Consolidated gravels are found between 10 and $50\,\mathrm{m}$ depth with a velocity of 750 up to $1000\,\mathrm{m/s}$. A velocity inversion occurs at $50\,\mathrm{m}$ depth due to the presence of lake sediments with velocity values going down to $500\,\mathrm{m/s}$. At $80\,\mathrm{m}$ depth, the velocity increases again asymptotically to $1000\,\mathrm{m/s}$ down to $250\,\mathrm{m}$ depth. The interface with Molasse rock is not clear but should appear around $100\,\mathrm{m}$. At $250\,\mathrm{m}$ depth, a major interface within the molasse is producing the fundamental peak in the ellipticity at $0.93\,\mathrm{Hz}$. $V_{s,30}$ is $579\,\mathrm{m/s}$. The ground type is B for EC8 [CEN, 2004] and E for SIA261 [SIA, 2003]. The theoretical SH transfer function and the impedance contrast of the quarter-wavelength velocity computed from the inverted profiles show moderate amplifications at some resonance frequencies. Recordings on the new station will allow to validate these simple 1D models.

Contents

1 Introduction

The station SZUZ (Zürich - Zeughaushof) is part of the Swiss Strong Motion Network (SSMNet). The city of Zürich has the largest exposure in Switzerland, but is located in a low hazard area. SZUZ has been installed in the framework of the SSMNet Renewal project in 2012 as a new site. This project includes also the site characterization. Passive array measurements have been selected as a standard tool to investigate these sites. An array measurement campaign was carried out on 21st February 2013 in the Zeughaushof and the streets around (Fig. 1), with a centre close to station SZUZ, in order to characterize the velocity profile under this station. This station is located in the Limmat basin, on the recent alluvia of the Sihl and the Limmat and on lake sediments. This report presents the measurement setup, the results of the H/V analysis and of the array processing of the surface waves (dispersion curves). Then, an inversion of these results into velocity profiles is performed. Standard parameters are derived to evaluate the amplification at this site.

Canton	City	Location	Station code	Site type	Slope
Zürich	Zürich	Zeughaushof	SZUZ	Deep valley	Flat

Table 1: Main characteristics of the study-site.

Figure 1: Picture of the site.

2 Geology

Station SZUZ was installed in the deepest part of the Limmat basin. According to gravimetry studies (Fig. 2), SZUZ is located in the centre of the basin and the quaternary sediments reach $120\,\mathrm{m}$ at this site, although this value is very uncertain. Only few boreholes are reaching the molasse bedrock in the basin. The borehole b 00-10069 (Fig. 3) reaches the Upper Freshwater molasse (OSM) at $97\,\mathrm{m}$ and was probably used to calibrate the depth from the gravimetric study.

Sediments at the surface on the geological map are fluvial sediments from the Sihl river. Details on the quaternary sediments are provided by other boreholes provided by the Amt für Abfall, Wasser, Energie und Luft of Kanton Zurich (see Fig. 4). They show a consistent layer of fluvial glacial sediments (mostly gravels) from the Limmat until $30 - 40\,\mathrm{m}$ depth and glacial lacustrine sediments (mostly silts) below. At borehole 421, the closest to station SZUZ, the upper layer is made of $10\,\mathrm{m}$ of unconsolidated washed moraine.

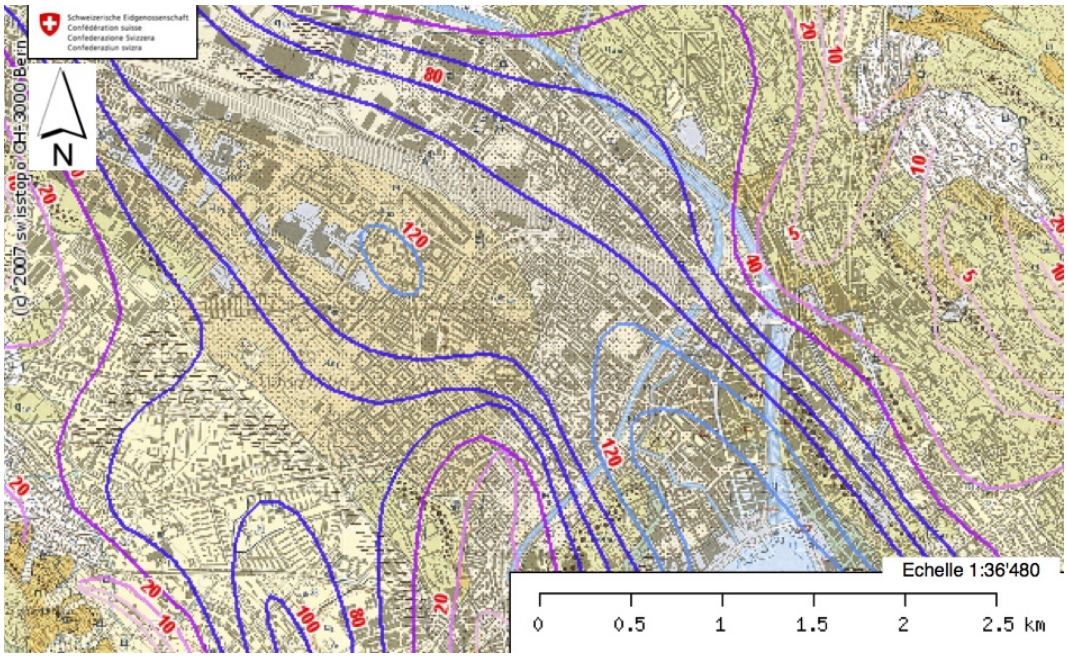

Figure 2: Depth of the Quaternary sediments according to a gravimetric study (geologieviewer.ch).

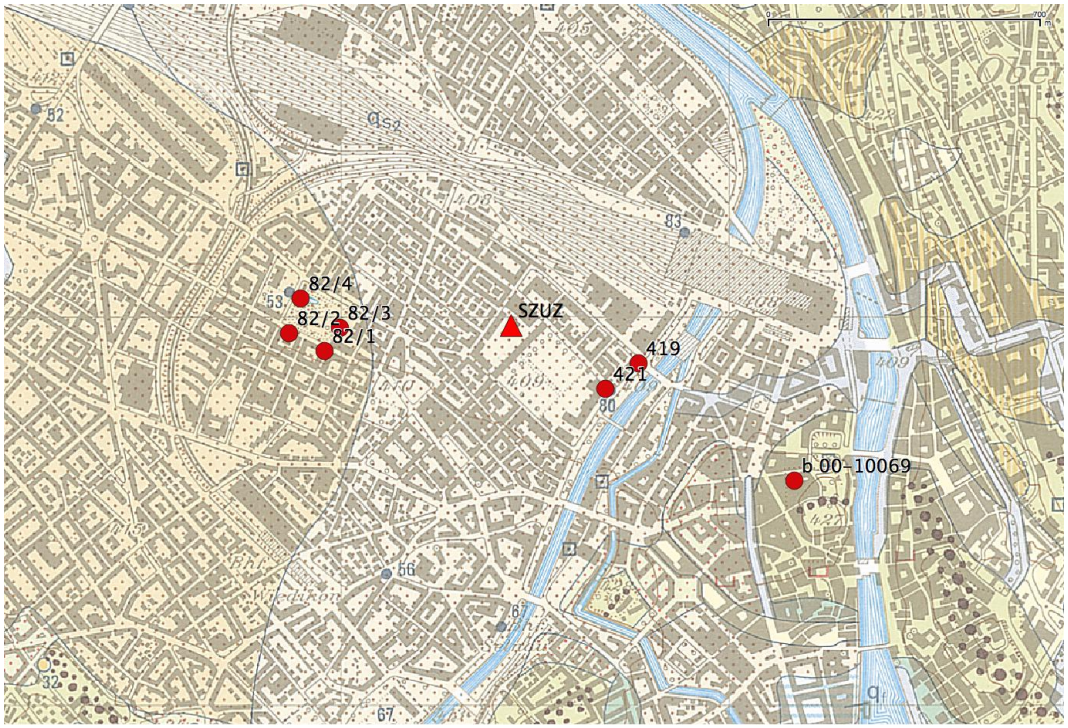

Figure 3: Boreholes (red points) overlaying the geological map.

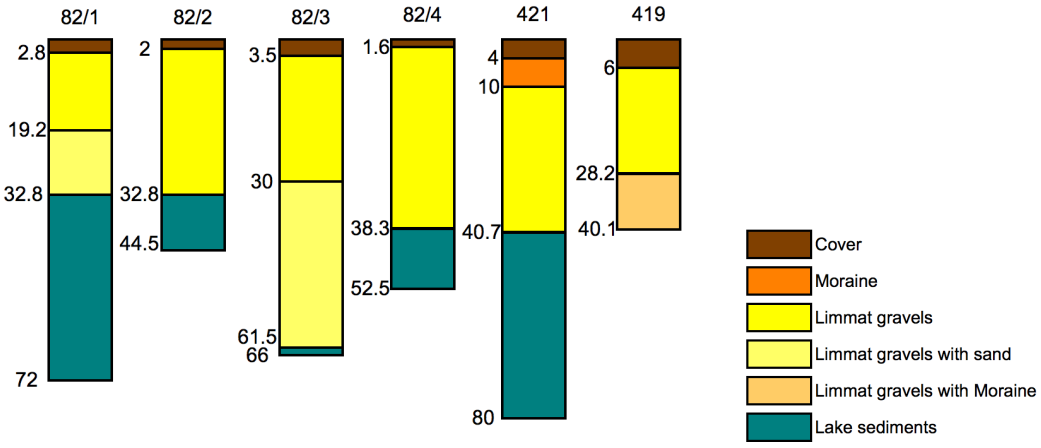

Figure 4: Schematic representation of the boreholes on Fig. 3 with depth in meters.

3 Experiment description

3.1 Ambient Vibrations

The ground surface is permanently subjected to ambient vibrations due to:

- natural sources (ocean and large-scale atmospheric phenomena) below $1\,\mathrm{Hz}$,
- local meteorological conditions (wind and rain) at frequencies around $1\,\mathrm{Hz}$,
- human activities (industrial machines, traffic…) at frequencies above $1\,\mathrm{Hz}$ [Bonnefoy-Claudet et al., 2006].

The objective of the measurements is to record these ambient vibrations and to use their propagation properties to infer the underground structure. First, the polarization of the recorded waves (H/V ratio) is used to derive the resonance frequencies of the soil column. Second, the arrival time delays at many different stations are used to derive the velocity of surface waves at different frequencies (dispersion). The information (H/V, dispersion curves) is then used to derive the properties of the soil column using an inversion process.

3.2 Equipment

For these measurements 12 Quanterra Q330 dataloggers named NR01 to NR12 and 14 Lennartz 3C 5 s seismometers were available (see Tab. 2). Each datalogger can record on 2 ports A (channels EH1, EH2, EH3 for Z, N, E directions) and B (channels EH4, EH5, EH6 for Z, N, E directions). Time synchronization was ensured by GPS. The sensors were placed on a metal tripod, in a $20\,\mathrm{cm}$ deep hole, when possible, for better coupling with the ground.

Digitizer	**Model**	**Number**	**Resolution**
	Quanterra Q330	12	$24\,\mathrm{bits}$
Sensor type	**Model**	**Number**	**Cut-off frequency**
Velocimeter	Lennartz 3C	14	$0.2\,\mathrm{Hz}$

Table 2: Equipment used.

3.3 Geometry of the arrays

Two array configurations were used, for a total of 4 rings of 10, 30, 75 and $150\,\mathrm{m}$ radius around a central station. The first configuration includes the 3 inner rings with 14 sensors; the second configuration includes the 2 outer rings (plus 2 sensors of the first ring) with 13 sensors. The minimum inter-station distance and the aperture are therefore 10 and $150\,\mathrm{m}$ and 10 and $300\,\mathrm{m}$, respectively. The experimental setup is displayed in Fig. 5. The final usable datasets are detailed in section 4.2.

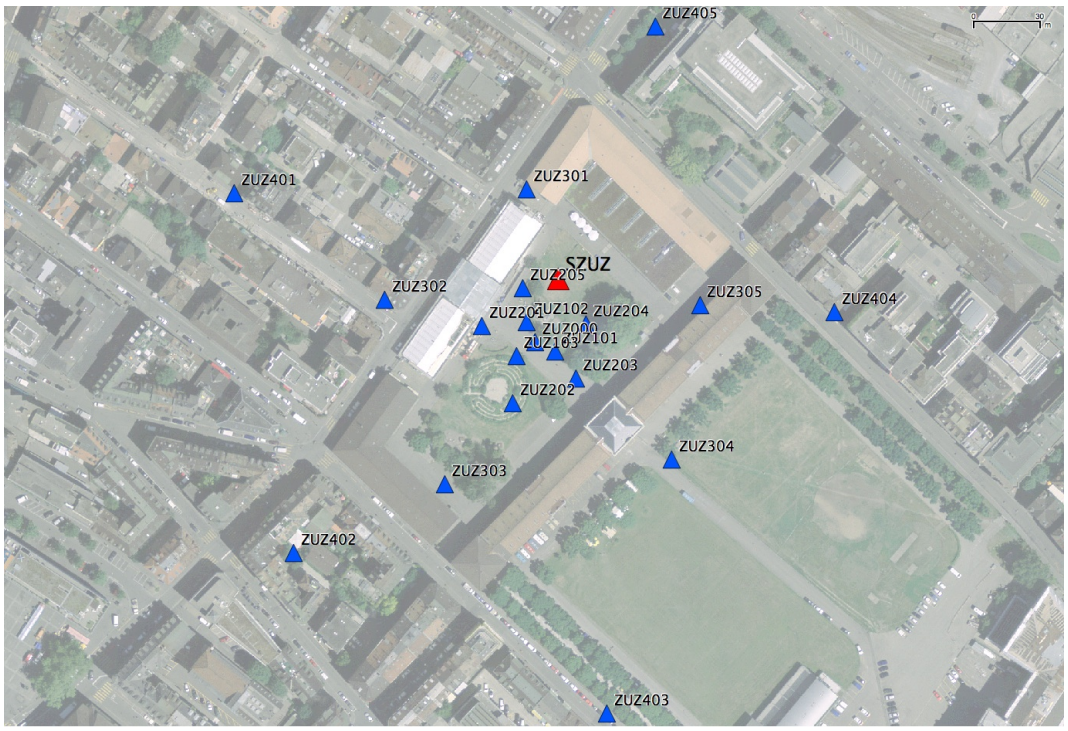

Figure 5: Geometry of the arrays.

3.4 Positioning of the stations

The sensor coordinates were measured using a differential GPS device (Leica Viva GS10), including only a rover station and using the Real Time Kinematic technique provided by Swisstopo. It allows an absolute positioning with an accuracy better than $5\,\mathrm{cm}$ on the Swissgrid. However, this accuracy was not reached at some points (ZUZ301 with $12\,\mathrm{cm}$, ZUZ302 with $41\,\mathrm{cm}$ and ZUZ305 with $33\,\mathrm{cm}$). For the outer ring, GPS raw-data logging allowed to improve the precision of points ZUZ401 to 405 using post-processing with the software Leica Geo-Office and a RINEX Virtual Reference downloaded from the Swisstopo server. After this post-processing, these points reached the $5\,\mathrm{cm}$ accuracy.

4 Data quality

4.1 Usable data

The largest time windows were extracted, for which all the sensors of the array were correctly placed and the GPS synchronization was ensured. The array was limited in size by the train station in the North. The quality of the datasets is surprisingly outstanding, probably because no sensor was close to a road with heavy nor rapid traffic (no effect of the air flow on the sensor). Moreover, as it turns out in the FK analysis, the noise of the city is not capable of reaching higher depth than around $10\,\mathrm{m}$ and is therefore seen only above $10\,\mathrm{Hz}$. However, two series of spurious peaks around 3.6 and $4.4\,\mathrm{Hz}$ are noticed.

Orientations of the sensors were checked by maximizing the correlation with the central station at low frequencies [Poggi et al., 2012b]. Deviations lower than $9\,^\circ$ were found for all points but ZUZ102 ($10\,^\circ$) and especially ZUZ305 ($15\,^\circ$). Original and rotated datasets are available for the 3C array analysis.

The characteristics of the datasets are detailed in Tab. 3.

4.2 Data processing

The data were first converted to SAC format including in the header the coordinates of the point (CH1903 system), the recording component and a name related to the position. The name is made of 3 letters characterizing the location (ZUZ here), 1 digit for the ring and 2 more digits for the number in the ring. Recordings were not corrected for instrumental response.

Dataset	Starting Date	Time	Length	F_s	Min. inter-distance	Aperture	# of points
1	2013/02/21	08:59	123 min	200 Hz	10 m	150 m	14
2	2013/02/21	11:57	154 min	200 Hz	10 m	300 m	13

Table 3: Usable datasets.

5 H/V processing

5.1 Processing method and parameters

In order to process the H/V spectral ratios, several codes and methods were used. The classical H/V method was applied using the Geopsy `http://www.geopsy.org` software. In this method, the ratio of the smoothed Fourier Transform of selected time windows are averaged. Tukey windows (cosine taper of 5% width) of $50\,\mathrm{s}$ long overlapping by 50% were selected. Konno and Ohmachi [1998] smoothing procedure was used with a b value of 60. The classical method computed using the method of Fäh et al. [2001] was also performed.

Moreover, the time-frequency analysis method [Fäh et al., 2009] was used to estimate the ellipticity function more accurately using the Matlab code of V. Poggi. In this method, the time-frequency analysis using the Wavelet transform is computed for each component. For each frequency, the maxima over time (10 per minute with at least $0.1\,\mathrm{s}$ between each) in the TFA are determined. The Horizontal to Vertical ratio of amplitudes for each maximum is then computed and statistical properties for each frequency are derived. A Cosine wavelet with parameter 9 is used. The mean of the distribution for each frequency is stored. For the sake of comparison, the time-frequency analysis of Fäh et al. [2001], based on the spectrogram, was also used, as well as the wavelet-based TFA coded in Geopsy.

The ellipticity extraction using the Capon analysis [Poggi and Fäh, 2010] (see section on array analysis) was also performed.

Method	Freq. band	Win. length	Anti-trig.	Overlap	Smoothing
Standard H/V Geopsy	$0.2-20\,\mathrm{Hz}$	$50\,\mathrm{s}$	No	50%	K&O 60
Standard H/V D. Fäh	$0.2-20\,\mathrm{Hz}$	$30\,\mathrm{s}$	No	75%	-
H/V TFA Geopsy	$0.2-20\,\mathrm{Hz}$	Morlet m=8 fi=1	No	-	-
H/V TFA D. Fäh	$0.2-20\,\mathrm{Hz}$	Specgram	No	-	-
H/V TFA V. Poggi	$0.2-20\,\mathrm{Hz}$	Cosine wpar=9	No	-	No

Table 4: Methods and parameters used for the H/V processing.

5.2 Results

All points show the same shape in their H/V below $10\,\mathrm{Hz}$ with a clear fundamental peak at $0.93\,\mathrm{Hz}$. A more variable second peak is found above and is mapped on Fig. 8.

Moreover, all the methods to compute H/V ratios are compared at the array centre on Fig. 7, in which the classical methods were divided by $\sqrt{2}$ to correct from the Love wave contribution [Fäh et al., 2001]. The classical and TFA methods match well at high frequencies but the fundamental peak value and amplitude vary for each method. The 3C FK analysis (Capon method) does not have resolution down to the peak but matches approximately at high frequency. The second peak is shifted towards higher frequencies compared to the centre of the array, though.

The fundamental peak at the SZUZ station is therefore at $0.93\,\mathrm{Hz}$, with a peak amplitude around 4 for the TFA methods.

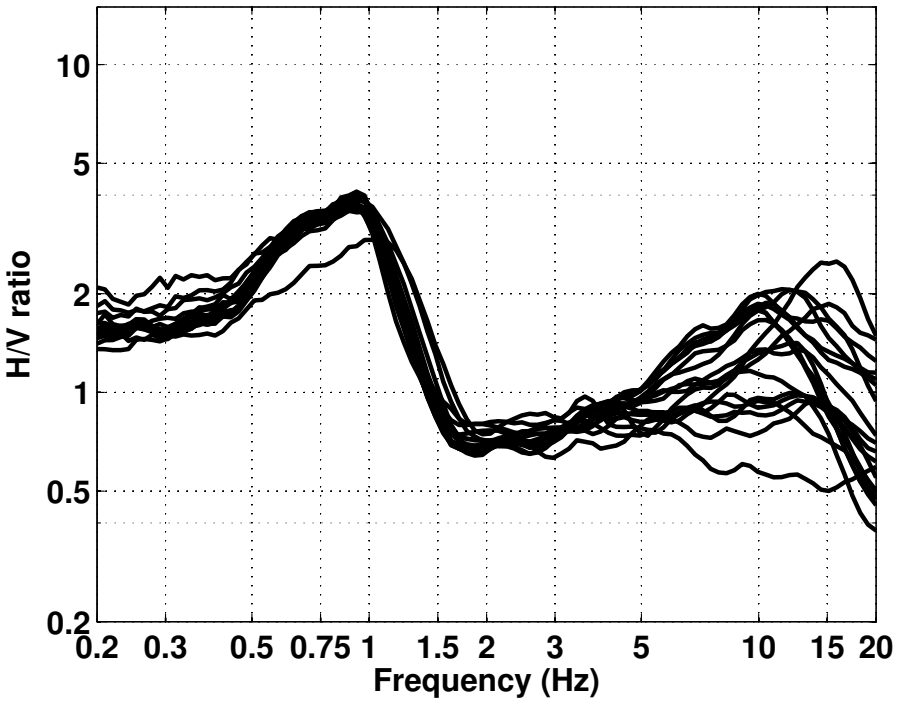

Figure 6: H/V spectral ratios (time-frequency analysis code V. Poggi).

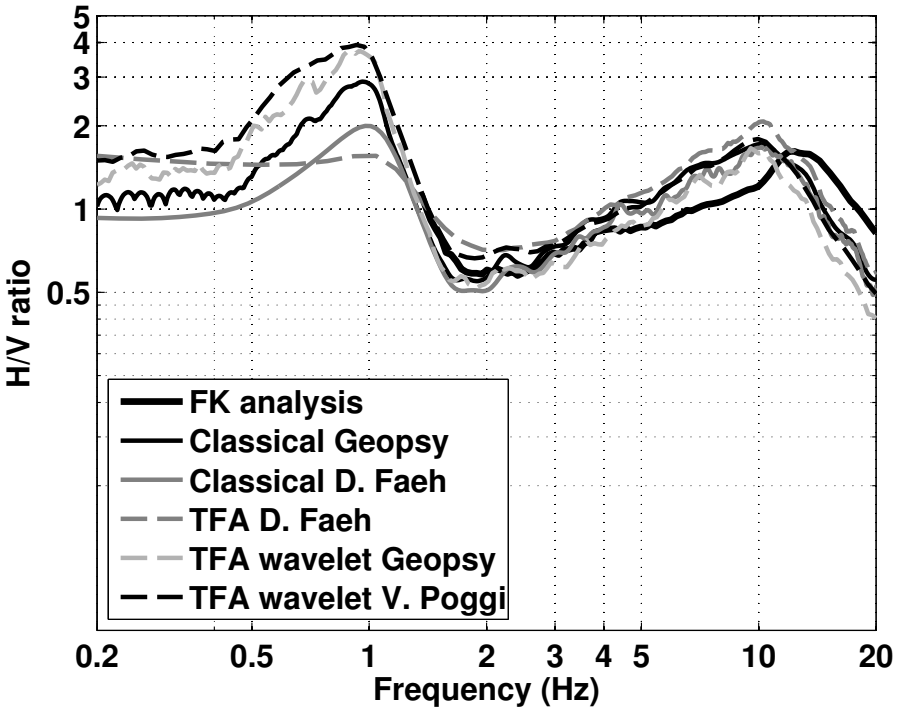

Figure 7: H/V spectral ratios for point ZUZ000 using the different codes. Classical methods were divided by $\sqrt{2}$.

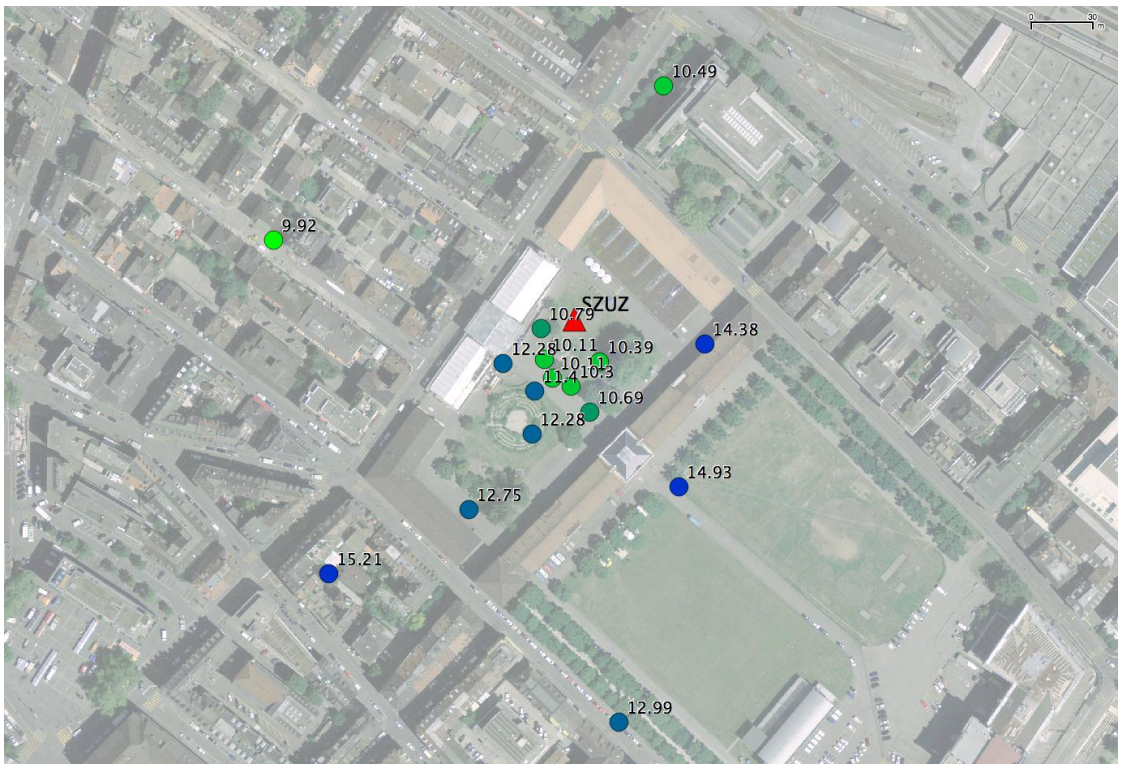

Figure 8: Map of the second peak in the H/V in the array with frequencies in Hz.

5.3 Polarization analysis

Considering the shape of the Limmat basin, a 2D resonance could occur. Therefore, polarization analysis on the array data was performed using the method of Burjánek et al. [2010]. All points (Fig. 9) show a weak polarization at $0.9\,\mathrm{Hz}$ perpendicularly to the valley axis (NE-SW). It is unlikely to be related to a 2D resonance.

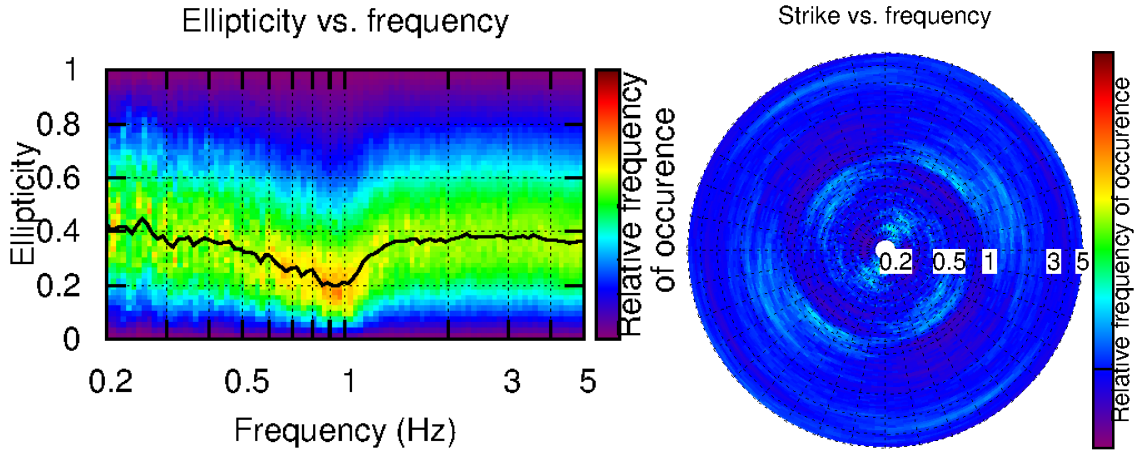

Figure 9: Polarization analysis at point ZUZ000. Left: Ellipticity (A trough in the ellipticity corresponds to polarized motion). Right: Strike of the polarization.

6 Array processing

6.1 Processing methods and parameters

The vertical components of the arrays were processed using the FK and the High-resolution FK analysis [Capon, 1969] using the Geopsy `http://www.geopsy.org` software. Better results were obtained using large time windows (300T). The results of computations of both datasets were merged to estimate the dispersion curves.

Moreover, a 3C array analysis [Fäh et al., 2008] was also performed using the array_tool_3C software [Poggi and Fäh, 2010]. It allows to derive Rayleigh and Love modes including the Rayleigh ellipticity. The results of computations of both datasets were merged to estimate the dispersion curves.

Method	Set	Freq. band	Win. length	Anti-trig.	Overlap	Grid step	Grid size	# max.
HRFK 1C	1	$1-25\,\mathrm{Hz}$	$300T$	No	50%	0.001	0.6	5
HRFK 1C	2	$1-25\,\mathrm{Hz}$	$300T$	No	50%	0.001	0.6	5
HRFK 3C	1	$1-20\,\mathrm{Hz}$	Wav. 10	No	50%	300	2000	5
			Tap. 0.2			m/s	m/s	
HRFK 3C	2	$1-20\,\mathrm{Hz}$	Wav. 10	No	50%	300	2000	5
			Tap. 0.2			m/s	m/s	

Table 5: Methods and parameters used for the array processing.

6.2 Obtained dispersion curves

The first Rayleigh mode in the 1C FK analysis could be picked between 1.5 and $13\,\mathrm{Hz}$ (Fig. 10) including its standard deviation. The velocities are ranging from $1200\,\mathrm{m/s}$ at $1.5\,\mathrm{Hz}$ down to $530\,\mathrm{m/s}$ at $13\,\mathrm{Hz}$. A higher mode can also be picked but is less certain.

Using the 3C analysis, both fundamental Rayleigh and Love modes can be picked (Fig. 11). Rayleigh fundamental mode is picked on the same frequency band as in the 1C analysis and Love from 1.2 to $15\,\mathrm{Hz}$. A higher Rayleigh mode is picked on a short frequency band as well.

All picked curves are presented together on Fig. 12. There are surprising differences in the picking of the different modes. The picked higher Rayleigh mode is the same in both methods. The fundamental Rayleigh is also similarly picked on both datasets and using both methods, except for the dataset 1 (3C analysis), where high frequencies are shifted towards higher velocities. It appears on Fig. 11 that the standard deviation is higher on this part of the curve. It may be due to the mixing of the fundamental and the first higher mode. Moreover, the picked Love curves are quite different for the first and second datasets. Except between 2.5 and $3.5\,\mathrm{Hz}$, the second dataset provides a low standard deviation, whereas the first shows a more scattered picture. Again, it may be due to the mixing with the first higher mode. Only the parts with low scatter have been kept. The picked higher Rayleigh mode was considered as the second higher mode.

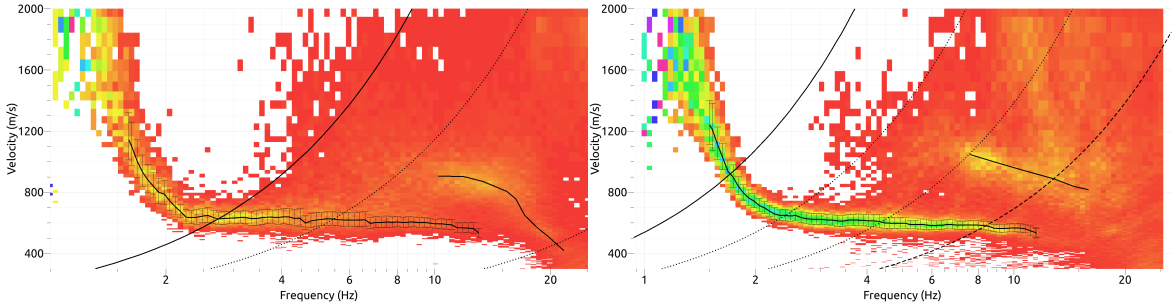

Figure 10: Dispersion curves obtained from the 1C array analysis (left: dataset 1; right: dataset 2).

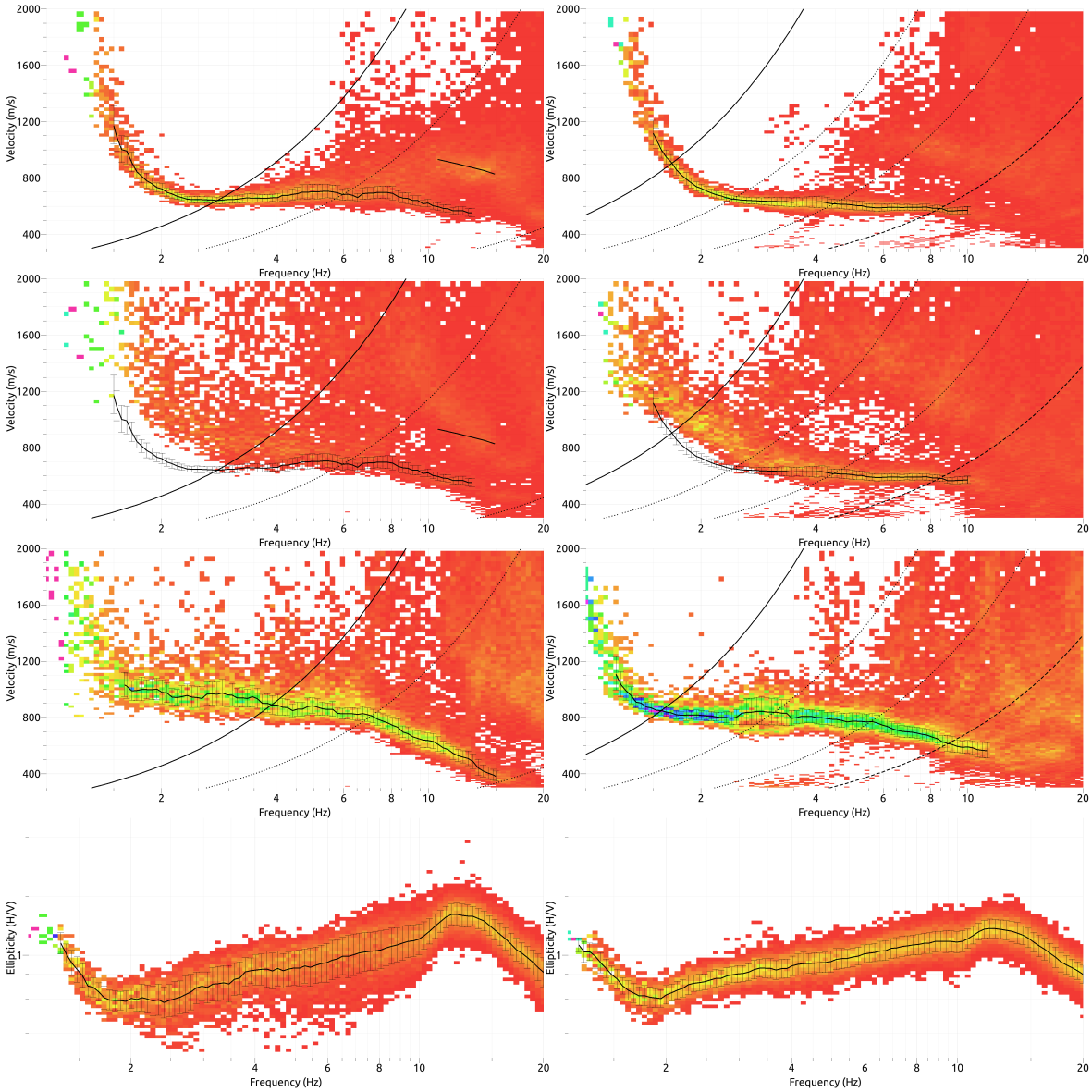

Figure 11: Dispersion curves and ellipticity obtained from the 3C array analysis (left: dataset 1; right: dataset 2; from top to bottom: vertical, radial, transverse components and ellipticity).

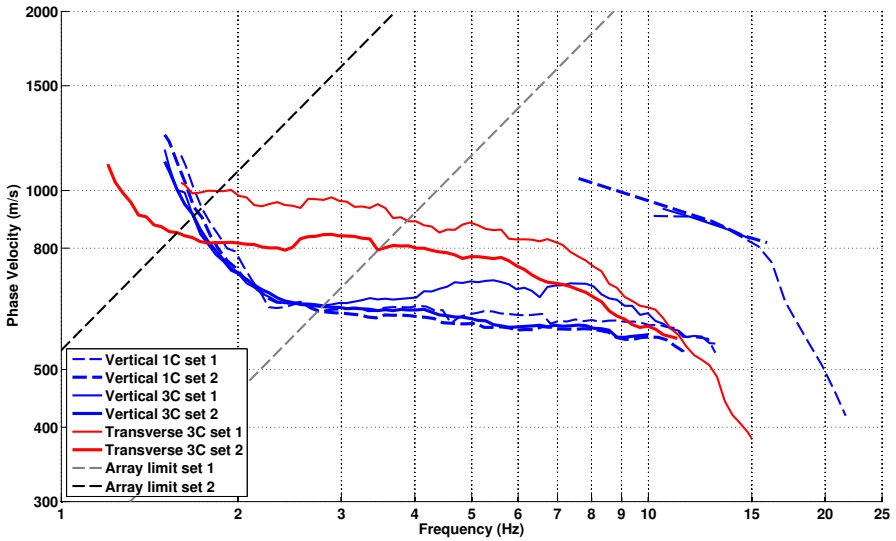

Figure 12: Picked dispersion curves from 1C and 3C FK methods.

7 Inversion and interpretation

7.1 Inversion

For the inversion, Rayleigh and Love fundamental and Rayleigh second higher modes dispersion curves, as well as the right flank of the ellipticity and the fundamental frequency at $0.93\,\mathrm{Hz}$ were used as simultaneous targets without standard deviation to avoid different weighting. The right flank of the second peak for the central point of the array was used as well to constrain better the upper part of the profiles. A weight of 0.2 was assigned to the ellipticity curve and the ellipticity peak. All curves were resampled using 50 points between 0.8 and $25\,\mathrm{Hz}$ in log scale.

The inversion was performed using the Improved Neighborhood Algorithm (NA) Wathelet [2008] implemented in the Dinver software. In this algorithm, the tuning parameters are the following: Ns_0 is the number of starting models, randomly distributed in the parameter space, Nr is the the number of best cells considered around these Ns_0 models, Ns is the number of new cells generated in the neighborhood of the Nr cells (Ns/Nr per cell) and It_{max} is the number of iteration of this process. The process ends with $Ns_0 + Nr * \frac{Ns}{Nr} * It_{max}$ models. The used parameters are detailed in Tab. 6.

It_{max}	Ns_0	Ns	Nr
500	10000	100	100

Table 6: Tuning parameters of Neighborhood Algorithm.

According to geology (section 2), stiff gravels are sitting on top of lake sediments so that a velocity inversion is expected at a depth of 30 to $60\,\mathrm{m}$. Therefore, low velocity zones were allowed in this depth range. The Poisson ratio was inverted in each layer in the range 0.2-0.4, up to 0.47 in the expected gravel layer, i.e. within the groundwater table. The density was assumed, using borehole data, between 2000 and $2500\,\mathrm{kg/m^3}$. Inversions with free layer depths as well as fixed layer depths were performed. 4 layers are enough to explain most of the targets (dispersion and ellipticity), but more layers are used to smooth the obtained results and better explore the parameter space. 5 independent runs of 5 different parametrization schemes (5 and 6 layers over a half space and 11, 12 and 13 layers with fixed depth) were performed. For further elaborations, the best models of these 25 runs were selected (Fig. 16).

A first layer of approximately $10\,\mathrm{m}$ is found with a low velocity 250 to $500\,\mathrm{m/s}$ (Fig. 13 and Fig. 16). It corresponds to unconsolidated recent sediments of the Sihl and the Limmat and washed moraine. It is responsible for the second peak in the ellipticity around $10\,\mathrm{Hz}$. As for the borehole data, consolidated material is found below $10\,\mathrm{m}$ with a velocity of 750 up to nearly $1000\,\mathrm{m/s}$ at $50\,\mathrm{m}$ depth. The velocity inversion occurs approximately at this depth with velocity values going down to $500\,\mathrm{m/s}$. It is however not well constrained. At $80\,\mathrm{m}$ depth, the velocity increases again asymptotically to $1000\,\mathrm{m/s}$ down to $250\,\mathrm{m}$ depth. At this depth, a major interface is producing the fundamental peak in the ellipticity. The velocity below this interface is however not constrained by these measurements. It is unlikely that this interface corresponds to the roof of the molasse. According to the gravimetric anomaly, the molasse should not be much deeper than $100\,\mathrm{m}$. Indeed, at this depth, the velocity would already correspond to molasse rock. The interface found at $250\,\mathrm{m}$ could be the Upper Freshwater Molasse (OSM)/Upper

Marine Molasse (OMM) interface. Indeed, this interface was found slightly below $300\,\mathrm{m}$ in the deep geothermal borehole of Triemli.

When comparing to the target curves (Fig. 14 and Fig. 15), the Rayleigh fundamental mode is well represented. The second higher mode, very uncertain, is compatible with the inversion. The fundamental Love mode is not fitting perfectly and may actually be mixed partly with its first higher mode as previously explained.

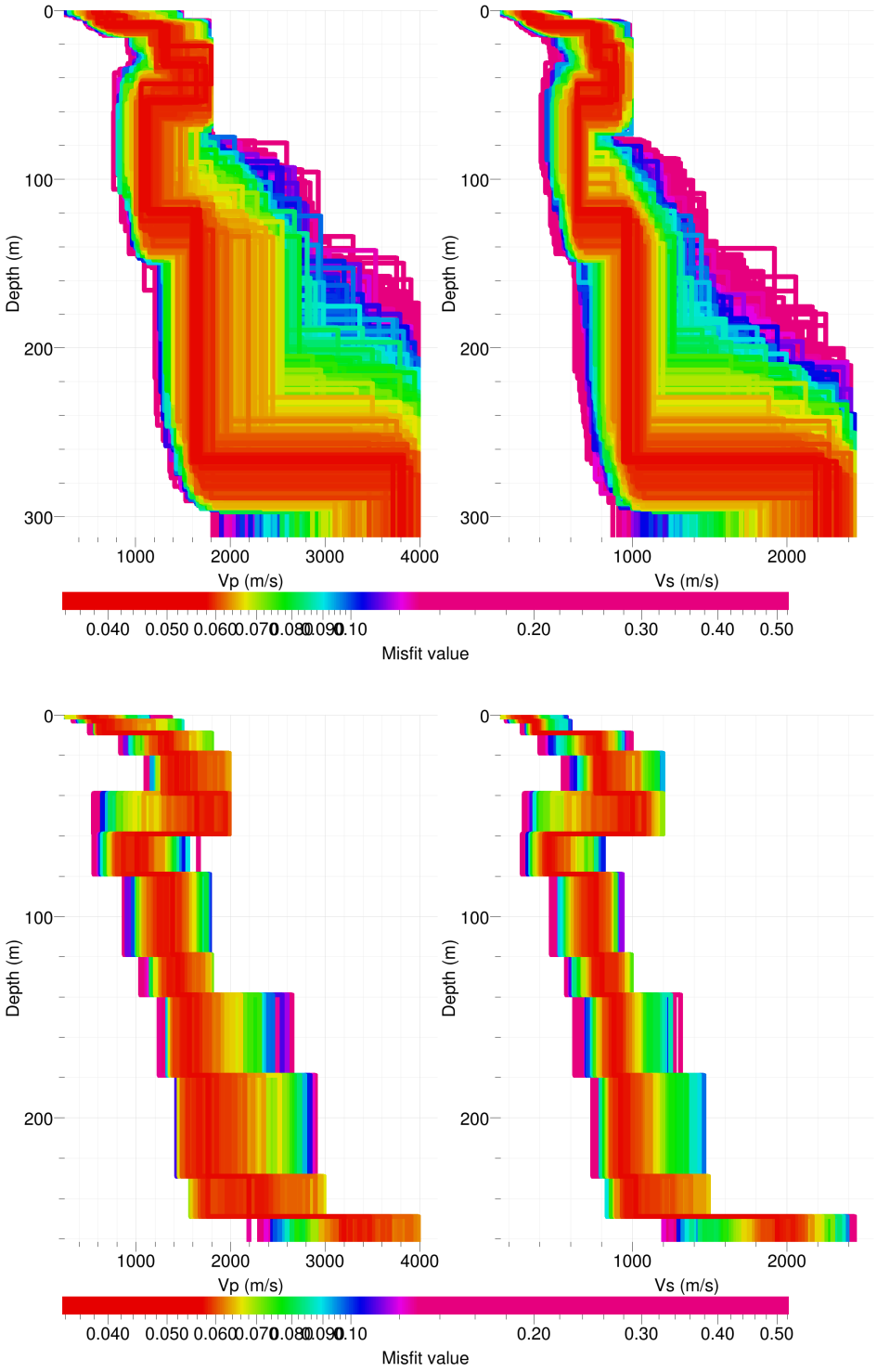

Figure 13: Inverted ground profiles in terms of V_p and V_s; top: free layer depth strategy; bottom: fixed layer depth strategy.

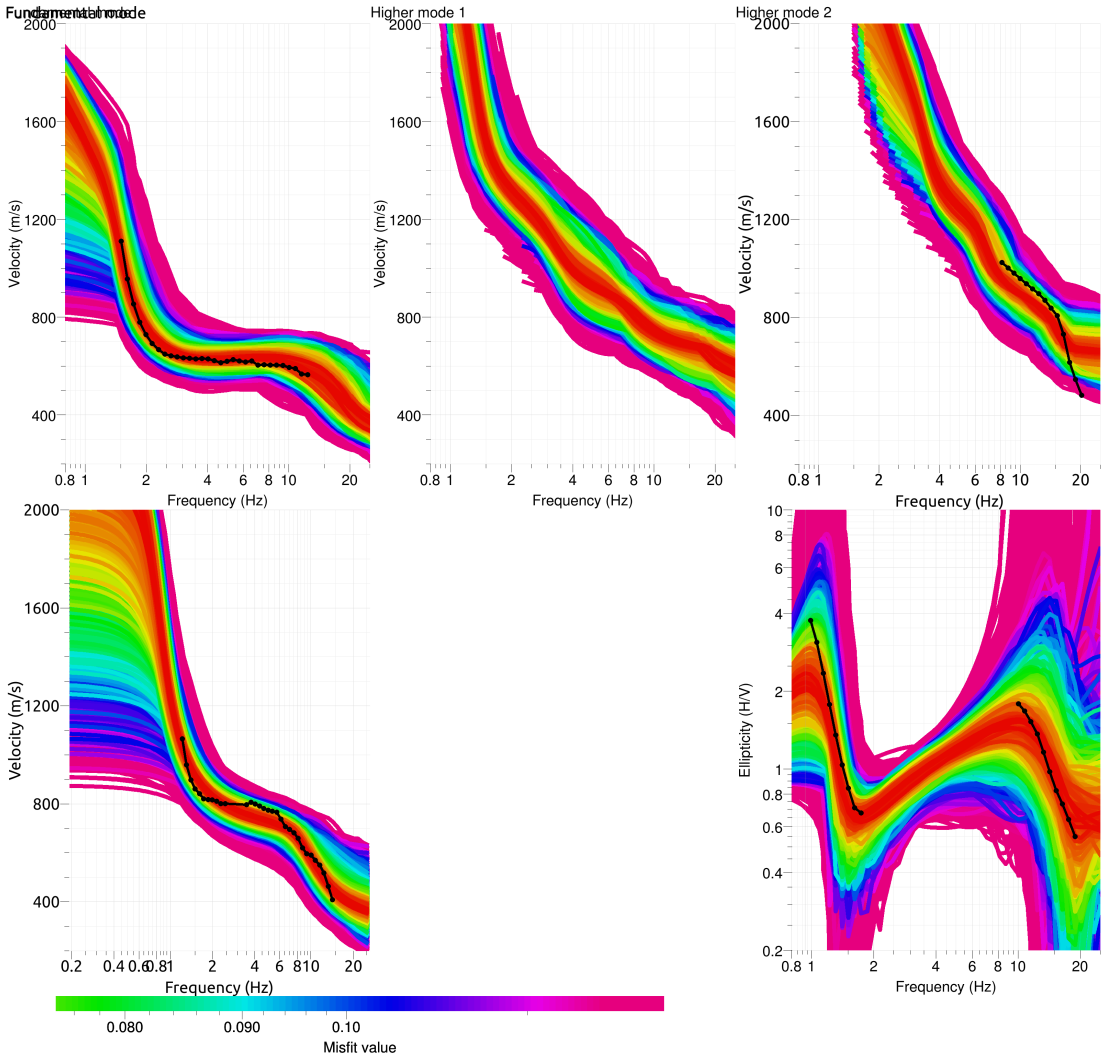

Figure 14: Comparison between inverted models and measured Rayleigh and Love modes and corresponding ellipticity, free layer depth strategy.

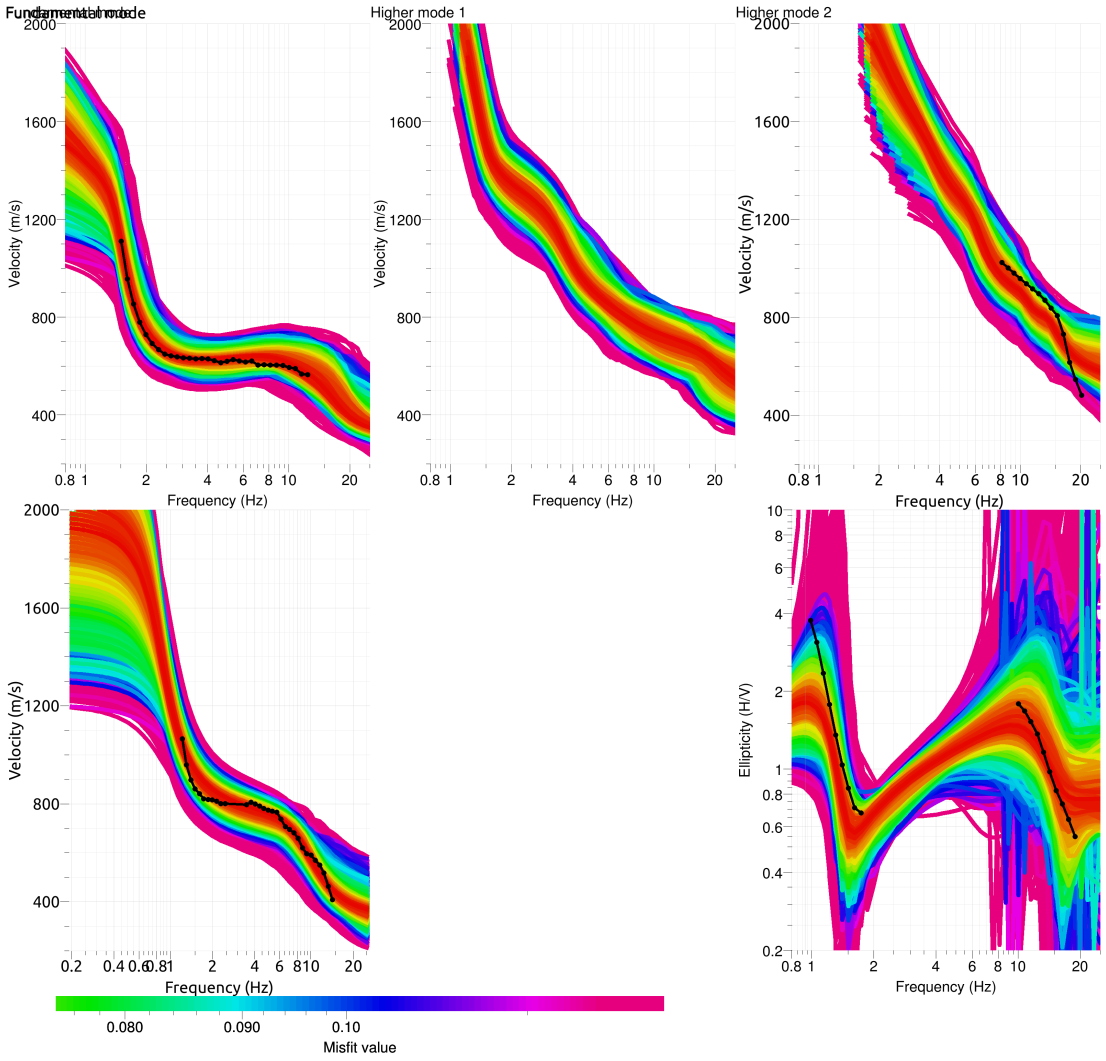

Figure 15: Comparison between inverted models and measured Rayleigh and Love modes and corresponding ellipticity, fixed layer depth strategy.

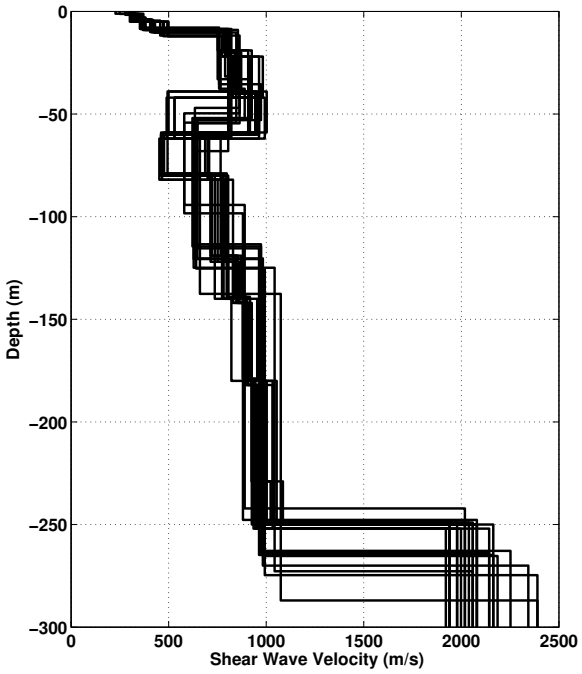

Figure 16: V_s ground profiles for the selected 25 best models.

7.2 Travel time average velocities and ground type

The distribution of the travel time average velocities at different depths was computed from the selected models. The uncertainty, computed as the standard deviation of the distribution of travel time average velocities for the considered models, is also provided, but its meaning is doubtful. $V_{s,30}$ is found to be $579\,\mathrm{m/s}$, which corresponds to class B in the Eurocode 8 [CEN, 2004]. For SIA261 [SIA, 2003], the first $10\,\mathrm{m}$ at $250 - 500\,\mathrm{m/s}$ on consolidated sediments at nearly $800\,\mathrm{m/s}$ put this site in ground type E. This is not the case for EC8 because less than $5\,\mathrm{m}$ are below $360\,\mathrm{m/s}$ on the upper part.

7.3 SH transfer function and quarter-wavelength velocity

The quarter-wavelength velocity approach [Joyner et al., 1981] provides, for a given frequency, the average velocity at a depth corresponding to 1/4 of the wavelength of interest. It is useful to identify the frequency limits of the experimental data (minimum frequency in dispersion curves at $1.2\,\mathrm{Hz}$ and in the ellipticity curve at $1\,\mathrm{Hz}$ here). The results using this proxy show that the dispersion curves constrain the profiles down to $150\,\mathrm{m}$ and the ellipticity down to $190\,\mathrm{m}$ (Fig. 17). Moreover, the quarter wavelength impedance-contrast introduced by Poggi et al. [2012a] is also displayed in the figure. It corresponds to the ratio between two quarter-wavelength average velocities, respectively from the top and the bottom part of the velocity profile, at a given frequency [Poggi et al., 2012a]. It shows a trough (inverse shows a peak) at the resonance frequency.

	Mean (m/s)	**Uncertainty (m/s)**
$V_{s,5}$	325	11
$V_{s,10}$	372	7
$V_{s,20}$	502	8
$V_{s,30}$	579	10
$V_{s,40}$	629	13
$V_{s,50}$	656	20
$V_{s,100}$	651	10
$V_{s,150}$	697	7
$V_{s,200}$	746	9

Table 7: Travel time averages at different depths from the inverted models. Uncertainty is given as one standard deviation from the selected profiles.

Moreover, the theoretical SH-wave transfer function for vertical propagation [Roesset, 1970] is computed from the inverted profiles. It is compared to the quarter-wavelength amplification [Joyner et al., 1981] that however cannot take resonances into account (Fig. 18). In this case, the models are predicting a gentle amplification up to a factor of 3 at several resonance peaks.

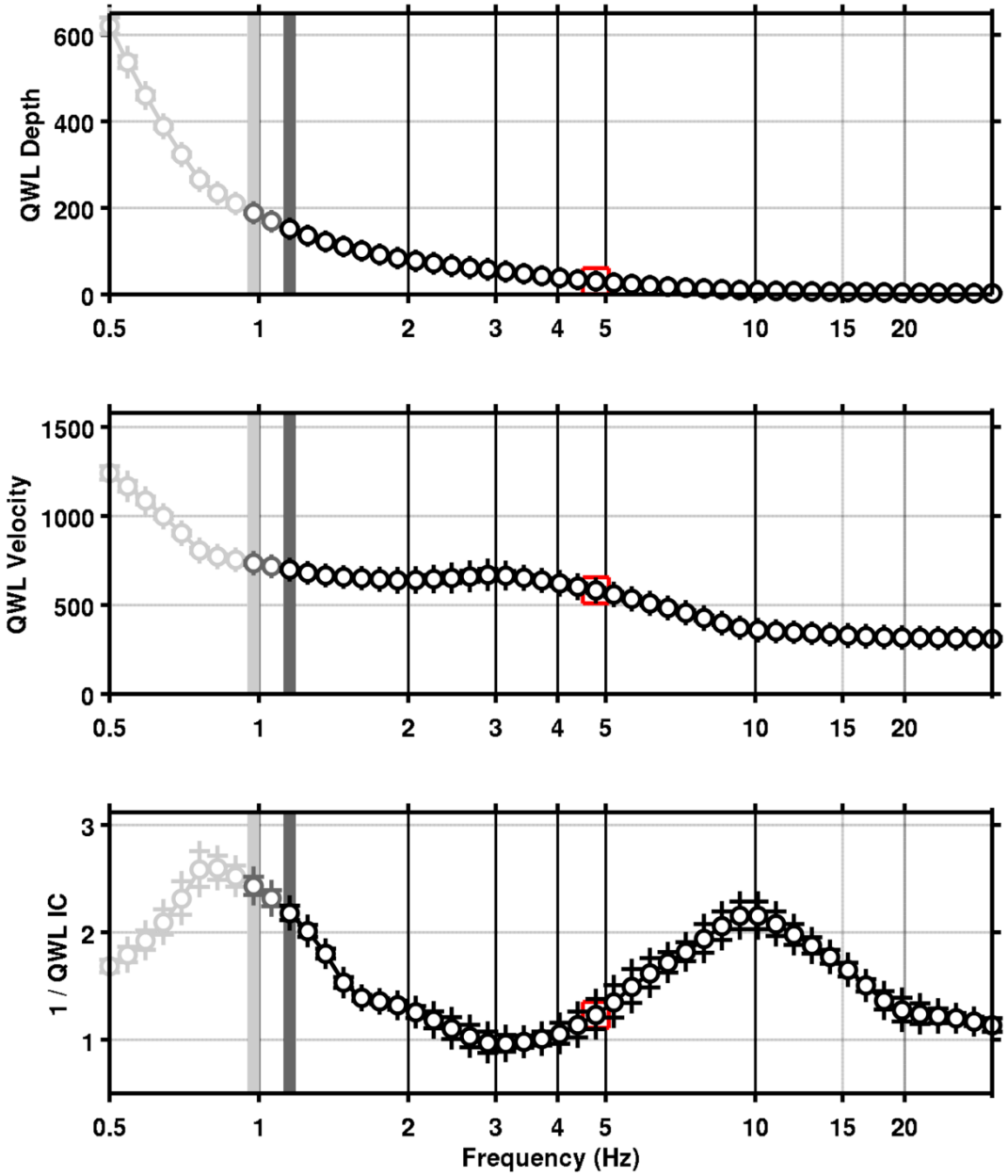

Figure 17: Quarter wavelength velocity representation of the velocity profile (top: depth, centre: velocity, bottom: inverse of the impedance contrast). Black curve is constrained by the dispersion curves, light grey is not constrained by the data. Red square is corresponding to $V_{s,30}$.

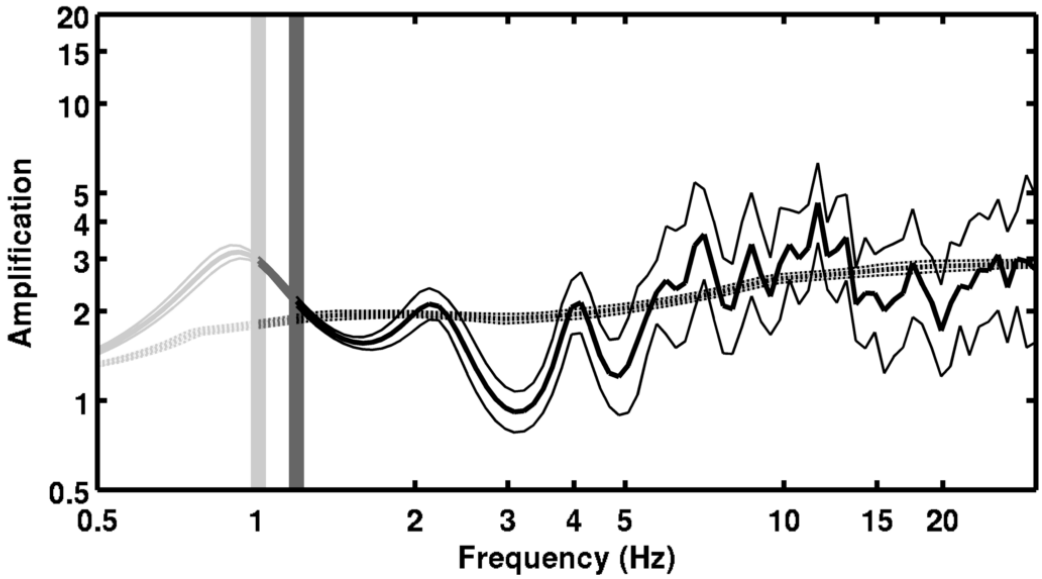

Figure 18: Theoretical SH transfer function (solid line) and quarter wavelength impedance contrast (dashed line) with their standard deviation. Significance of the greyshades is detailed in Fig. 17.

8 Conclusions

The array measurements presented in this study were successful in deriving a velocity model for the site of the SZUZ station. We found a first layer of approximately $10\,\mathrm{m}$ with velocities from 250 to $500\,\mathrm{m/s}$ corresponding to recent fluvial sediments and washed moraine. It is responsible for a peak in the ellipticity around $10\,\mathrm{Hz}$. Consolidated gravels are found between 10 and $50\,\mathrm{m}$ depth with a velocity of 750 up to $1000\,\mathrm{m/s}$. A velocity inversion occurs at this depth due to the presence of lake sediments with velocity values going down to $500\,\mathrm{m/s}$. At $80\,\mathrm{m}$ depth, the velocity increases again asymptotically to $1000\,\mathrm{m/s}$ down to $250\,\mathrm{m}$ depth. The interface with molasse is not clear but should appear around $100\,\mathrm{m}$. At $250\,\mathrm{m}$ depth, a major interface within the molasse is producing the fundamental peak in the ellipticity at $0.93\,\mathrm{Hz}$.
$V_{s,30}$ is $579\,\mathrm{m/s}$, which would corresponds to ground type B in the Eurocode 8 [CEN, 2004]. The site would be classified in ground type E for the SIA261 [SIA, 2003]. The theoretical 1D SH transfer function and impedance contrast of the quarter-wavelength velocity computed from the inverted profiles show moderate amplifications at some resonance frequencies. Recordings on the new station will allow to compare to these simple models.

Acknowledgements

The authors thank Anne Sauron, Franz Weber, Cyrill Bonjour and Laura Ermert for their help on short notice during these measurements.

References

Sylvette Bonnefoy-Claudet, Fabrice Cotton, and Pierre-Yves Bard. The nature of noise wavefield and its applications for site effects studies. *Earth-Science Reviews*, 79(3-4): 205–227, December 2006. ISSN 00128252. doi: 10.1016/j.earscirev.2006.07.004. URL http://linkinghub.elsevier.com/retrieve/pii/S0012825206001012.

Jan Burjánek, Gabriela Gassner-Stamm, Valerio Poggi, Jeffrey R. Moore, and Donat Fäh. Ambient vibration analysis of an unstable mountain slope. *Geophysical Journal International*, 180(2):820–828, February 2010. ISSN 0956540X. doi: 10.1111/j.1365-246X.2009.04451.x. URL http://doi.wiley.com/10.1111/j.1365-246X.2009.04451.x.

J. Capon. High-Resolution Frequency-Wavenumber Spectrum Analysis. *Proceedings of the IEEE*, 57(8):1408–1418, 1969.

CEN. *Eurocode 8: Design of structures for earthquake resistance - Part 1: General rules, seismic actions and rules for buildings*. European Committee for Standardization, en 1998-1: edition, 2004.

Donat Fäh, Fortunat Kind, and Domenico Giardini. A theoretical investigation of average H / V ratios. *Geophysical Journal International*, 145:535–549, 2001.

Donat Fäh, Gabriela Stamm, and Hans-Balder Havenith. Analysis of three-component ambient vibration array measurements. *Geophysical Journal International*, 172(1):199–213, January 2008. ISSN 0956540X. doi: 10.1111/j.1365-246X.2007.03625.x. URL http://doi.wiley.com/10.1111/j.1365-246X.2007.03625.x.

Donat Fäh, Marc Wathelet, Miriam Kristekova, Hans-Balder Havenith, Brigitte Endrun, Gabriela Stamm, Valerio Poggi, Jan Burjanek, and Cécile Cornou. Using Ellipticity Information for Site Characterisation Using Ellipticity Information for Site Characterisation. Technical report, NERIES JRA4 Task B2, 2009.

William B. Joyner, Richard E. Warrick, and Thomas E. Fumal. The effect of Quaternary alluvium on strong ground motion in the Coyote Lake, California, earthquake of 1979. *Bulletin of the Seismological Society of America*, 71(4):1333–1349, 1981.

Katsuaki Konno and Tatsuo Ohmachi. Ground-Motion Characteristics Estimated from Spectral Ratio between Horizontal and Vertical Components of Microtremor. *Bulletin of the Seismological Society of America*, 88(1):228–241, 1998.

Valerio Poggi and Donat Fäh. Estimating Rayleigh wave particle motion from three-component array analysis of ambient vibrations. *Geophysical Journal International*, 180(1):251–267, January 2010. ISSN 0956540X. doi: 10.1111/j.1365-246X.2009.04402.x. URL http://doi.wiley.com/10.1111/j.1365-246X.2009.04402.x.

Valerio Poggi, Benjamin Edwards, and D. Fah. Characterizing the Vertical-to-Horizontal Ratio of Ground Motion at Soft-Sediment Sites. *Bulletin of the Seismological Society of America*, 102(6):2741–2756, December 2012a. ISSN 0037-1106. doi: 10.1785/0120120039. URL http://www.bssaonline.org/cgi/doi/10.1785/0120120039.

Valerio Poggi, Donat Fäh, Jan Burjanek, and Domenico Giardini. The use of Rayleigh-wave ellipticity for site-specific hazard assessment and microzonation: application to the city of Lucerne, Switzerland. *Geophysical Journal International*, 188(3):1154–1172, March 2012b. ISSN 0956540X. doi: 10.1111/j.1365-246X.2011.05305.x. URL http://doi.wiley.com/10.1111/j.1365-246X.2011.05305.x.

J.M. Roesset. Fundamentals of soil amplification. In R. J. Hansen, editor, *Seismic Design for Nuclear Power Plants*, pages 183–244. M.I.T. Press, Cambridge, Mass., 1970. ISBN 978-0-262-08041-5. URL http://mitpress.mit.edu/catalog/item/default.asp?ttype=2\&tid=5998.

SIA. *SIA 261 Actions sur les structures porteuses*. Société suisse des ingénieurs et des architectes, Zürich, sia 261:20 edition, 2003.

Marc Wathelet. An improved neighborhood algorithm: Parameter conditions and dynamic scaling. *Geophysical Research Letters*, 35(9):1–5, May 2008. ISSN 0094-8276. doi: 10.1029/2008GL033256. URL http://www.agu.org/pubs/crossref/2008/2008GL033256.shtml.